Acta Cryst. (1962). **15**, 770

Stacking Faults and Two New Modifications of the Laves Phase in Mg-Cu-Al System

BY YUKITOMO KOMURA

Faculty of Science, Osaka City University, Sugimotocho, Sumiyoshi-ku, Osaka, Japan

(*Received* 15 *August* 1961)

A ternary Laves phase, having a composition of approximately MgCuAl, was examined by the X-ray method. Diffuse scattering and superstructure reflections were observed between strong reflections due to C_{14} (2-layer type) and C_{36} (4-layer type).

Two new types of modification were found from the superstructure reflections; one is expressed by a rhombohedral 9-layer sequence such as $AB'ABC'BCA'C$ or its reverse structure $A'CA'C'BC'B'AB'$, with a unit cell $a_0 = 12{\cdot}97$ Å, $\alpha = 22° 50'$, which corresponds to a hexagonal unit cell with $a_0 = 5{\cdot}14$, $c_0 = 37{\cdot}89$ Å. The other type is expressed by a hexagonal 5-layer sequence such as $ABCAB'$ or its reverse structure $AB'A'C'B'$, with $a_0 = 5{\cdot}14$, $c_0 = 21{\cdot}05$ Å. Layer symbols A and A' used here denote two kinds of puckered close-packed layers sandwiched between kagomé nets.

General features of X-ray diffuse scattering observed are satisfactorily explained by a mixture of 9-layer sequences with stacking faults and disordered stacking of two 5-layer sequences. An extension of a theory developed by Kakinoki & Komura for the case of close-packed structures is applied.

1. Introduction

Binary intermetallic compounds known as 'Laves phases' are reported to have the following three closely related structures: (1) The C_{14} structure, typified by the hexagonal phase $MgZn_2$, (2) the C_{15} structure, typified by the cubic phase $MgCu_2$ and (3) the C_{36} structure, typified by the hexagonal phase $MgNi_2$. The close relationship among these structures can be easily understood from a few good reviews (Raynor, 1949; Berry & Raynor, 1953). However, the construction of these structures will be explained in a later section more precisely based upon stacking of layers.

Laves & Witte (1936) investigated alloys lying along a section $MgCu_2$–$MgAl_2$ to see the effect of changing the electron/atom ratio. When copper is replaced by aluminium, the cubic $MgCu_2$ structure extends to about 1·80 electrons per atom, and is succeeded by the hexagonal $MgNi_2$ structure up to 2·07 electrons per atom at high temperatures, or 1·88 electrons per atom at low temperatures. The hexagonal $MgZn_2$ structure occurs between 1·88 and 2·15 electrons per atom at lower temperatures. Fig. 1 shows the schematic diagram of the structural change in these alloys.

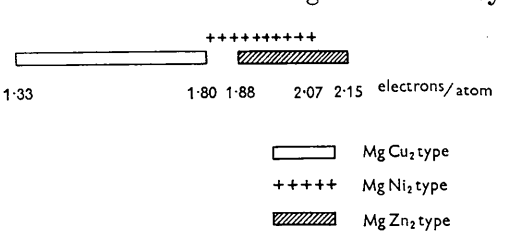

Fig. 1. Structural change of Mg–Cu–Al alloys as a function of electron/atom ratio.

From the inspection of Fig. 1 one can expect stacking faults to occur during the course of crystallization in the alloys of the system Mg–Cu–Al whose electron/atom ratios lie between 1·88 and 2·07, because, as mentioned above, the stability regions of two of the fundamental structures overlap at higher and lower temperatures in this range. In fact X-ray photographs of the alloys having their composition around this region showed not only strong reflections due to the fundamental C_{14} and C_{36} structures, but also diffuse scattering indicating stacking faults along the hexagonal c^* direction; in addition they showed several superstructure reflections between main reflections of C_{14} and C_{36}, which suggests existence of new modifications.

Methods for calculating X-ray intensities from crystals with stacking faults have been well established by several authors (Hendricks & Teller, 1942; Wilson, 1942; Jagodzinski, 1949*a*, *b*, *c*, 1954; Kakinoki & Komura, 1952, 1954*a*, *b*) in the case of close-packed structures.

The purpose of the present paper is to interpret the diffuse scattering observed in the Laves phase, MgCuAl, in terms of stacking faults by extending the method used previously (Kakinoki & Komura, 1954*b*), which enabled us to determine, further, the structures of two new modifications from superstructure reflections.

2. Experimentals

Alloys were prepared from pure magnesium (99·9%) and mother alloys which contained 50 at.% of copper and aluminium. The mother alloys were made in a kryptol furnace by mixing 99·99% aluminium with molten electrolytic copper. The composition was

checked by chemical analysis. They were then fused with pure magnesium in high alumina crucibles placed in a nichrome furnace at around 900 °C. and were allowed to cool slowly to room temperature. The preparation of ingots in vacuum was impossible because of the sublimation of magnesium, so that a flux ($MgCl_2$, NaCl and KCl mixture) was used in order to prevent oxidation of the alloys in the course of melting. Several alloys of Mg–Cu–Al, having their electron/atom ratios from 1·88 to 2·07, were made by melting accurately weighed quantities of magnesium, the mother alloys and, in addition, necessary amounts of copper and aluminium.

Preliminary X-ray powder photographs showed that these alloys were fairly homogeneous with no indication of the presence of any phase due to impurities. Well developed single crystals of hexagonal plate shape were found in the blow holes produced accidentally in ingots. Particular samples examined in the present paper have the electron/atom ratio 2·0 which corresponds to the chemical formula MgCuAl.

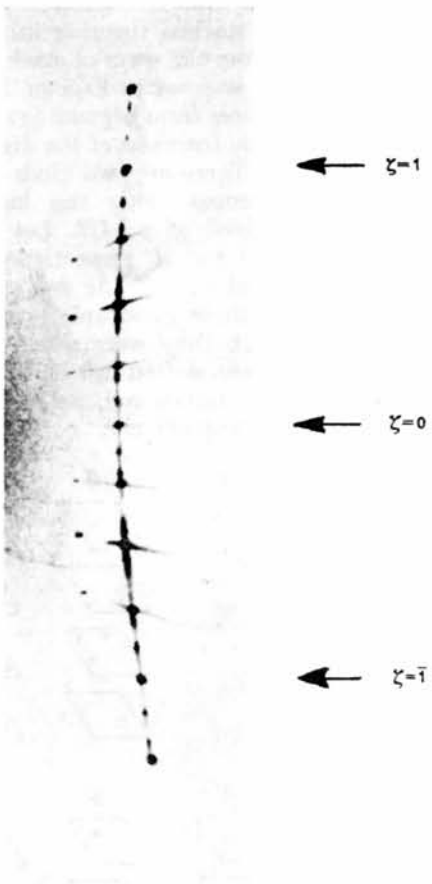

Fig. 2. 20ζ row line in an oscillation photograph about the c axis.

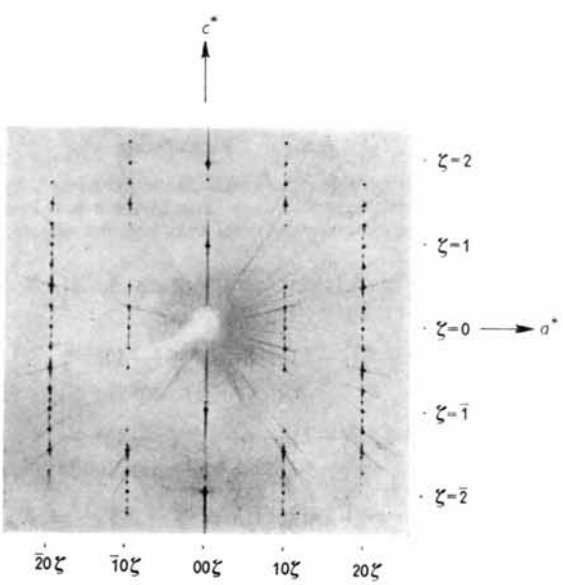

Fig. 3. Precession photograph of the $h0\zeta$ net.

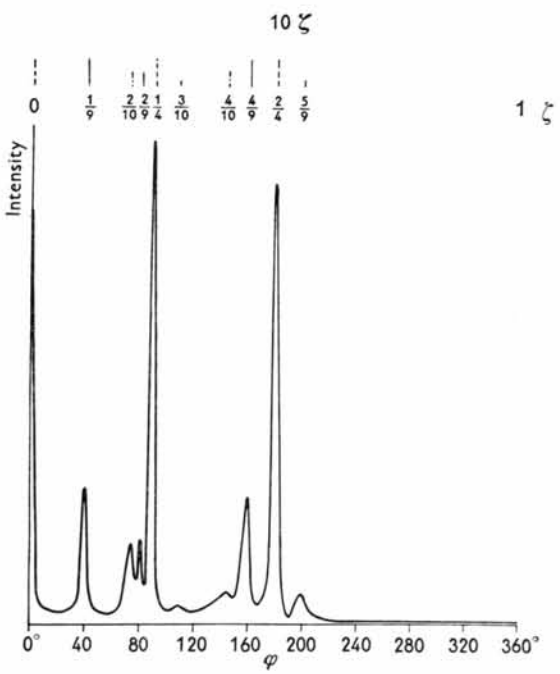

Fig. 4.

Laue, oscillation, Weissenberg and precession photographs were taken by Cu $K\alpha$ radiation using tiny fragments cut from single crystals of MgCuAl, their linear dimensions being around 0·2 mm. An oscillation photograph about the c axis and a precession photograph about the a axis are shown in Figs. 2 and 3 as examples. Strong diffuse scattering along c^* indicating stacking faults can be seen easily from these photographs as we expected. Superstructure reflections indicating new modifications are also recognized between main strong reflections which belong to the fundamental C_{14} and C_{36} structures. Intensity distributions of diffuse scattering along c^* were estimated by

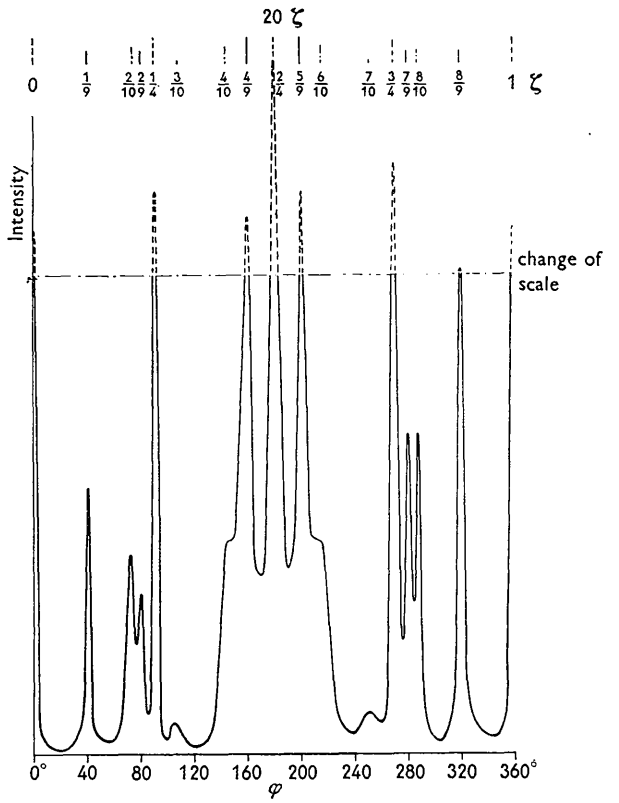

Fig. 5.

Figs. 4 and 5. Sketches of microphotometer traces for 10ζ and 20ζ row lines. Vertical lines shown in the upper part of the figures indicate the positions of Bragg reflections of the regular structures.

microphotometer traces. Since peaks or superstructure reflections were too intense to be estimated along with diffuse scattering from photometer traces, corrections were made by visual estimation using standard wedges. Sketches of these photometer traces for 10ζ and 20ζ row lines are given in Figs. 4 and 5, where ζ is the continuous co-ordinate along c^*. Here the period c is taken for a layer thickness, to be described in the next section, so that ζ is fractional for superstructure reflections.†

3. Analysis of the structures

(a) *Description of the structures as layer stacking*

In the structure of the Laves phases, there are two kinds of sheets; one is a denser layer forming kagomé (Frank & Kasper, 1959)—a net of triangles and hexagons. The other is found between these kagomé nets, and consists of three triangular nets of magnesium and other metals stacked together in a close-packed manner. Fig. 6 shows the ways of stacking these nets, the distance from kagomé to kagomé being taken as a unit, while distances from kagomé to each triangular net are indicated by fractions of the distance between two kagomé nets. There are two kinds of such stackings, their differences being the location of the triangular net placed at $z=1/2$. Let us call these quadruple layers A and A' respectively (Fig. 6), corresponding to Δ and ∇, in Frank & Kasper's notation (1959). Hereafter these quadruple layers will be referred to as though they were single layers. If the A and A' layers are shifted 1/3 or 2/3 in the $[\bar{1}10]$ direction of the hexagonal cell, we obtain B and B', or C and C' layers respectively.

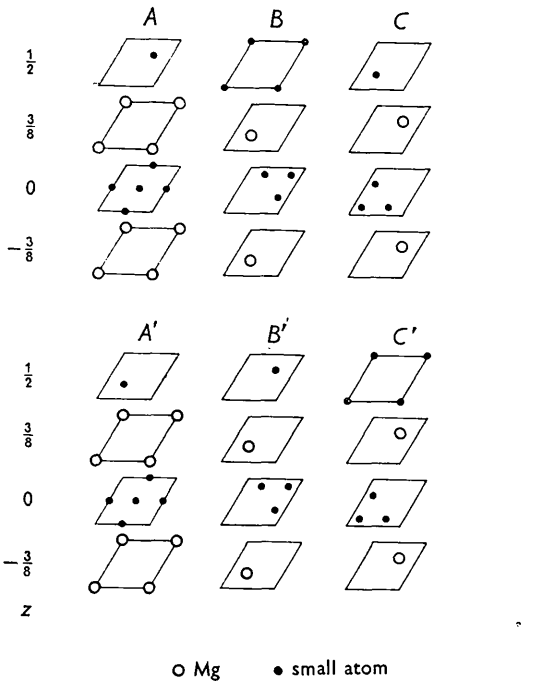

Fig. 6. Six fundamental layers which are constructed by a kagomé and three triangular nets. Parameter z is taken as a fraction of the distance between two kagomé sheets.

Referring to Fig. 6 layer form factors A, A', B, B', C and C' are given by

$$V_A = 2f_a \cos \tfrac{3}{8}\varphi + f_b[(-1)^h + (-1)^k + (-1)^{h-k}] + f_b\varepsilon \exp(i\varphi/2), \quad (1)\dagger$$

$$V_{A'} = 2f_a \cos \tfrac{3}{8}\varphi + f_b[(-1)^h + (-1)^k + (-1)^{h-k}] + f_b\varepsilon^* \exp(i\varphi/2), \quad (2)\dagger$$

$$V_B = V_A\varepsilon^*, \quad V_{B'} = V_{A'}\varepsilon^*, \quad V_C = V_A\varepsilon, \quad V_{C'} = V_{A'}\varepsilon, \quad (3)\dagger$$

† More precisely speaking, $(\mathbf{s}-\mathbf{s}_0)/\lambda$ can be expressed in terms of the basis vectors $\mathbf{a}^*$, $\mathbf{b}^*$, $\mathbf{c}^*$ reciprocal to $\mathbf{a}$, $\mathbf{b}$, $\mathbf{c}$, using ξ, η, ζ as continuous co-ordinates:

$$(\mathbf{s}-\mathbf{s}_0)/\lambda = \xi\mathbf{a}^* + \eta\mathbf{b}^* + \zeta\mathbf{c}^*,$$

where $\mathbf{s}_0$ and $\mathbf{s}$ are unit vectors along the incident and scattered directions, λ the incident wavelength. Since there is no disturbance in the regular arrangement within a layer, diffracted intensity can be observed only when $\xi=h$, $\eta=k$, h and k being any integer, but ζ continuous variable. Symbol $hk\zeta$ used here has the above meaning.

† For simplicity, two Laue functions regarding a and b directions in the layer plane are omitted.

where $\varepsilon=\exp(2\pi i(h-k)/3)$, phase shift $\varphi=2\pi\zeta$, f_a is the atomic form factor for magnesium and f_b that for smaller atom.

It should be mentioned here that when $h-k=3n$ (n integral), $\varepsilon=1$, hence

$$V_A=V_{A'}=V_B=V_{B'}=V_C=V_{C'}\,.$$

From this relation we obtain

$$I(h,\,h-3n,\,\zeta)=V_A^*V_A\sin^2\pi N_0\zeta/\sin^2\pi\zeta\,, \qquad (4)$$

irrespective of any stacking of A, A', B, B', C and C', N_o being the number of layers. Equation (4) gives maxima at $\zeta=$integer, in agreement with the characteristic features of X-ray photographs. This is the reason why such layers as shown in Fig. 6 are adopted.

On account of the spatial requirements of large magnesium atoms, for example, A can be followed only by B and B', the possible ways of layer stacking being shown in Table 1.

Table 1. *Possible ways of the layer stacking*

$A\langle{}^{B}_{B'}$	$A'\langle{}^{C}_{C'}$
$B\langle{}^{C}_{C'}$	$B'\langle{}^{A}_{A'}$
$C\langle{}^{A}_{A'}$	$C'\langle{}^{B}_{B'}$

Thus the fundamental three structures can be described as layer sequences. They are: AB' for C_{14}–$MgZn_2$ structure, ABC for C_{15}–$MgCu_2$ structure and $AB'A'C$ for C_{36}–$MgNi_2$ structure. We may call these three structures 2-layer, 3-layer and 4-layer types, respectively, from the point of view of layer stacking.

(*b*) *Observed reflections*

X-ray photographs of MgCuAl samples examined show the characteristic features for the row lines $h,\,h-3n,\,\zeta$ as mentioned before, but rather complicated features for other row lines as can be seen in Figs. 2 and 3. Strong Bragg reflections along other row lines are explained by the 4-layer type structure (2-layer type reflections are included), but several other superstructure reflections are found on the same row lines, which suggest the presence of new modifications.

To each reflection in Figs. 4 and 5 is assigned a fractional index, ζ, where the denominator is

$$\text{true } c_0 \text{ for this phase}/c \text{ for one layer}\,,$$

and the numerator is the regular Bragg index referred to the true c_0. This convention is adopted in order to count easily the number of layers in the repeating unit. From the figures one can see that these reflections correspond to a mixture of a 9-layer type structure and a weak 10-layer type structure.

By closer examination of reflections of higher order in h and k, it is found that these reflections are split into two groups, in addition to the separation due to $K\alpha_1$ and $K\alpha_2$ doublets. One of these groups belongs to the 4-layer type structure, and is not accompanied with any diffuse scattering along the c^* direction. The other group has a somewhat larger unit cell, and it contains all reflections due to the other modifications such as 2-layer, 9-layer and 10-layer structures. Diffuse scattering accompanies this second group. Lattice constants of these two sub-unit cells were evaluated as follows:

$a_0=5{\cdot}11$, $c=4{\cdot}17\pm0{\cdot}01$ Å, for the 4-layer structure,
$a_0=5{\cdot}14$, $c=4{\cdot}21\pm0{\cdot}01$ Å, for other modifications,

where c was taken as one layer thickness for the sake of comparison. From these observations it was concluded that there were at least two different kinds of crystallites, their corresponding axes being parallel with each other. One of these has a perfectly regular 4-layer type structure, so that we will omit consideration of this kind hereafter. Since there are several modifications, the Bragg index l cannot be used in common for the different periods of the c axis, and attention is called to the index ζ so defined that identity period for the c direction is one layer in thickness.

(*c*) *Structure of the* 9*-layer sequence*

Reflections due to the 9-layer sequence should be generally found at $\zeta=p/9$, p being any integer, but in the present case they are characterized by the following rules: (1) For $h-k=3n$ (n integral), only $\zeta=0,\,1,\,2$, etc., can be found (equation (4)). (2) For $h-k=3n\pm1$, $\zeta=3p/9$ are not observed. (3) Reflections including diffuse scattering are symmetrical with respect to $\zeta=0$. From these observations the crystal must be a mixture of equal amounts of two rhombohedral cells, having the same structure but oppositely oriented. On the other hand it is concluded from Table 1 that the rhombohedral cells of 9-layer type are only $AB'ABC'BCA'C$ and $A'CA'C'BC'B'AB'$. So the crystal should be a mixture of them.

By using equations (1), (2) and (3) structure factors of the two rhombohedral sequences can be expressed as the following equations:

For $AB'ABC'BCA'C$

$$F_1=(1+\varepsilon^*\exp(i3\varphi)+\varepsilon\exp(i6\varphi))\times(V_A+V_{B'}\exp(i\varphi)+V_A\exp(i2\varphi))\,, \qquad (5)$$

for $A'CA'C'BC'B'AB'$

$$F_2=(1+\varepsilon\exp(i3\varphi)+\varepsilon^*\exp(i6\varphi))(V_{A'}+V_C\exp(i\varphi)+V_{A'}\exp(i2\varphi))\,, \qquad (6)$$

in which f_b in equations (1) and (2) is taken a mean of the atomic form factors of copper and aluminium,

since it is assumed here that copper and aluminium are randomly distributed among the positions where smaller atoms should be. Comparisons are made in Fig. 7 for the observed and calculated intensities of 10ζ and 20ζ reflections as representative examples; agreements between these values are fairly good.† Diffuse scattering accompanying these reflections will be discussed in the next section.

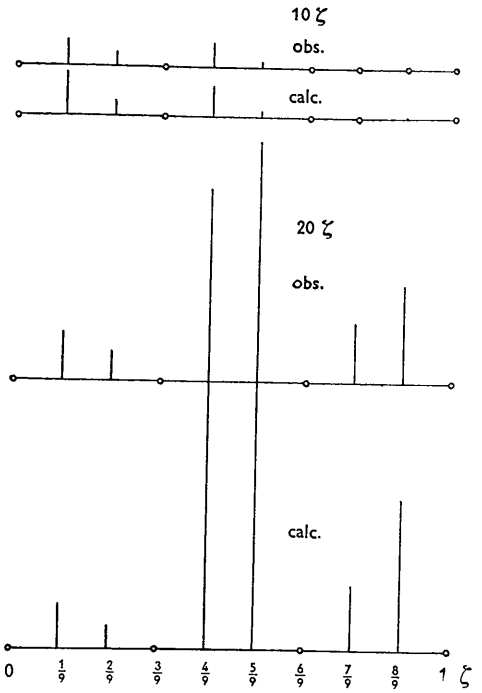

Fig. 7. Comparison of the observed and calculated intensities of the 10ζ and 20ζ reflections as a mixture of two regular 9-layer structures $AB'ABC'BCA'C$ and $A'CA'C'BC'B'AB'$.

Reflections located very close to $\zeta=2/9$ and $7/9$ which are measured as 2/10 and 8/10, and the accompanying broad maxima at around $\zeta=3/10$, $4/10$, $6/10$ and $7/10$, are designated as a sort of disordered stacking between two 5-layer sequences of $ABCAB'$ and $AB'A'C'B'$. The reason for this is that the spacings of those reflections correspond to a 10-layer sequence and especially odd multiples of $1/10$ of ζ are rather diffuse. The detailed discussions will be given in a later section.

4. Interpretation of diffuse scattering

The diffuse scattering accompanying the Bragg reflections is observed extending along the c^* direction, except for $h-k=3n$, where only sharp reflections are found at integral values for ζ. Such a feature of the diffuse scattering can be interpreted as the effect of stacking faults. The solution of this problem will be given as an improvement of the matrix method (Kakinoki & Komura, 1954*b*) which has been applied to the case of close-packed structures.

† Lorentz and polarization corrections do not differ so greatly from reflection to reflection in the range we consider, that these corrections are neglected at the present stage.

(*a*) 9-*layer sequence with stacking faults*

Intensity distributions of the diffuse scattering along c^* have maxima at positions corresponding to the 9-layer structure. These broad maxima extend to maxima corresponding to the 2-layer structure, so that let us consider first the stacking faults of the 9-layer sequence which is mixed slightly with the 2-layer structure during the course of crystallization. Many authors call this sort of disorder the growth fault. In order to make up a **P** matrix such as shown in equation (7), three layers are coupled so that the 9-layer and 2-layer structures may be found for extreme cases.

$$\mathbf{P}=\begin{array}{c|cc:cc:cc} & AB'A & A'CA' & BC'B & B'AB' & CA'C & C'BC' \\ \hline AB'A & & & 1-\delta & \delta & & \\ A'CA' & & & & & \delta & 1-\delta \\ \hdashline BC'B & & & & & 1-\delta & \delta \\ B'AB' & \delta & 1-\delta & & & & \\ \hdashline CA'C & 1-\delta & \delta & & & & \\ C'BC' & & & \delta & 1-\delta & & \end{array}, \tag{7}$$

in which the st-element indicates the probability of finding the layer of t-kind after that of s-kind, and blank positions of this matrix are all zero which means, for instance, $AB'A$ layer can not be followed by anyone of the other layers except for $BC'B$ and $B'AB'$ layers as seen from Table 1. An extreme case when $\delta=0$ corresponds to the mixture of the two regular 9-layer structures

$$AB'ABC'BCA'C \quad \text{and} \quad A'CA'C'BC'B'AB'.$$

On the other hand when $\delta=1$, the regular 2-layer structure $AB'AB'AB'\ldots$ (which is equivalent to the structure $A'CA'CA'C\ldots$) is obtained. In this sense we may call δ a stacking fault probability of 9-layer sequence.

The general intensity equation for X-rays diffracted by a disordered crystal can be given by (Kakinoki & Komura, 1952, 1954*b*)

$$I=N\,\text{spur}\,\mathbf{VF}+\sum_{m=1}^{N-1}(N-m)\,\text{spur}\,\mathbf{VFP}^m\exp(-im\varphi)+\text{conjugate}, \tag{8}$$†

where **V** and **F** matrices are in this case as follows:

$$\mathbf{V}=\begin{pmatrix} \mathbf{v} & \varepsilon^*\mathbf{v} & \varepsilon\mathbf{v} \\ \varepsilon\mathbf{v} & \mathbf{v} & \varepsilon^*\mathbf{v} \\ \varepsilon^*\mathbf{v} & \varepsilon\mathbf{v} & \mathbf{v} \end{pmatrix}, \quad \mathbf{v}=\begin{pmatrix} V_1^*V_1 & V_1^*V_2 \\ V_2^*V_1 & V_2^*V_2 \end{pmatrix}. \tag{9}$$

† The diffracted intensity I is measured in electron unit.

$$\mathbf{F}=\tfrac{1}{3}\begin{pmatrix}\mathbf{w} & 0 & 0\\ 0 & \mathbf{w} & 0\\ 0 & 0 & \mathbf{w}\end{pmatrix},\qquad \mathbf{w}=\begin{pmatrix}w_1 & 0\\ 0 & w_2\end{pmatrix}. \tag{10}$$

Here, V_1 and V_2 are the layer form factors of coupled three layers of $AB'A$ and $A'CA'$ respectively, so that their expressions are derived from equations (1), (2) and (3) as

$$\begin{aligned}V_1&=V_A+V_{B'}\exp(i\varphi)+V_A\exp(i2\varphi)\\&=V_A+V_{A'}\varepsilon^*\exp(i\varphi)+V_A\exp(i2\varphi),\end{aligned} \tag{11}$$

$$\begin{aligned}V_2&=V_{A'}+V_C\exp(i\varphi)+V_{A'}\exp(i2\varphi)\\&=V_{A'}+V_A\varepsilon\exp(i\varphi)+V_{A'}\exp(i2\varphi).\end{aligned} \tag{12}$$

In equation (10), the $\mathbf{F}$ matrix is expressed in the same way as in the close-packed structure, $\frac{1}{3}w_1$ and $\frac{1}{3}w_2$ being the probabilities of finding coupled layers of $AB'A$ and $A'CA'$ at any jth layer respectively. Since the layers having their origins at (0, 0, 0), $(\frac{2}{3}, \frac{1}{3}, 0)$ and $(\frac{1}{3}, \frac{2}{3}, 0)$ can be thought as equivalent to each other, the $\mathbf{F}$ matrix is divided by the three identical minor matrices, as shown in equation (10). In the case of growth fault w_1 and w_2 can be taken as equal; i.e., $w_1=w_2=\frac{1}{2}$ unless $\delta=0$. The phase shift due to a coupled layer was taken as three times that of a single layer. The $\mathbf{P}$ matrix may be put in an abbreviated form as follows:

$$\mathbf{P}=\begin{pmatrix}0 & \mathbf{p} & \mathbf{p}'\\ \mathbf{p}' & 0 & \mathbf{p}\\ \mathbf{p} & \mathbf{p}' & 0\end{pmatrix},\quad \text{where}\quad \begin{aligned}\mathbf{p}&=\begin{pmatrix}1-\delta & \delta\\ 0 & 0\end{pmatrix}\\ \mathbf{p}'&=\begin{pmatrix}0 & 0\\ \delta & 1-\delta\end{pmatrix}\end{aligned}. \tag{13}$$

It can easily be shown that spur $\mathbf{VFP}^m$ can be reduced to a rather simpler form when $\mathbf{V}, \mathbf{F}, \mathbf{P}$ are substituted by equations (9), (10) and (13), as follows:

$$\begin{aligned}&\text{spur }\mathbf{VFP}^m\\&=\tfrac{1}{3}\,\text{spur}\begin{pmatrix}\mathbf{v} & \varepsilon^*\mathbf{v} & \varepsilon\mathbf{v}\\ \varepsilon\mathbf{v} & \mathbf{v} & \varepsilon^*\mathbf{v}\\ \varepsilon^*\mathbf{v} & \varepsilon\mathbf{v} & \mathbf{v}\end{pmatrix}\begin{pmatrix}\mathbf{w} & 0 & 0\\ 0 & \mathbf{w} & 0\\ 0 & 0 & \mathbf{w}\end{pmatrix}\begin{pmatrix}0 & \mathbf{p} & \mathbf{p}'\\ \mathbf{p}' & 0 & \mathbf{p}\\ \mathbf{p} & \mathbf{p}' & 0\end{pmatrix}^m\\&=\text{spur }\mathbf{vw}(\varepsilon\mathbf{p}+\varepsilon^*\mathbf{p}')^m.\end{aligned} \tag{14}$$

When the matrix $(\varepsilon\mathbf{p}+\varepsilon^*\mathbf{p}')$ is diagonalized, then spur $\mathbf{vw}(\varepsilon\mathbf{p}+\varepsilon^*\mathbf{p}')^m$ can be written as

$$\text{spur }\mathbf{vw}(\varepsilon\mathbf{p}+\varepsilon^*\mathbf{p}')^m=\sum_{\nu=1}^{S}c_\nu x_\nu^m, \tag{15}$$

where x_ν's are the elements of the diagonalized matrix of $(\varepsilon\mathbf{p}+\varepsilon^*\mathbf{p}')$. Hence, x_ν's can be obtained by solving the following characteristic equation,

$$\det(\varepsilon\mathbf{p}+\varepsilon^*\mathbf{p}'-x\mathbf{1})=\begin{vmatrix}\varepsilon(1-\delta)-x & \varepsilon\delta\\ \varepsilon^*\delta & \varepsilon^*(1-\delta)-x\end{vmatrix}=0. \tag{16}$$

Also c_ν's in equation (15) are obtained by solving the following simultaneous equations:

$$\begin{aligned}c_1+c_2&=\text{spur }\mathbf{vw}=\tfrac{1}{2}(V_1^*V_1+V_2^*V_2)\\x_1c_1+x_2c_2&=\text{spur }\mathbf{vw}(\varepsilon\mathbf{p}+\varepsilon^*\mathbf{p}')\\&=\tfrac{1}{2}\{\varepsilon(1-\delta)V_1^*V_1+\varepsilon^*\delta V_1^*V_2+\varepsilon\delta V_2^*V_1\\&\quad+\varepsilon^*(1-\delta)V_2^*V_2\},\end{aligned} \tag{17}$$

where $\mathbf{w}$ is taken as $w_1=w_2=\frac{1}{2}$ as mentioned before. Thus the intensity formula (8) can be written more simply by the use of the above relationships as follows:

$$\begin{aligned}I=(N/2)(V_1^*V_1+V_2^*V_2)+\sum_{m=1}^{N-1}(N-m)\\\times\exp(-im3\varphi)\sum_{\nu=1}^{2}c_\nu x_\nu^m+\text{conjugate},\end{aligned} \tag{18}$$

where N is the number of coupled layers in the crystal, hence $3N=N_0$.

Thus the results obtained from equation (18) are summarized as follows:

(1) For $h-k=3n$,

$$I=V^*V\sin^2 N\tfrac{3}{2}\varphi/\sin^2\tfrac{3}{2}\varphi, \tag{19}$$

where

$$\begin{aligned}V=V_1=V_2=(1+\exp(i\varphi)+\exp(i2\varphi))\\\times\{2f_a\cos\tfrac{3}{8}\varphi+f_b[(-1)^h+(-1)^k+(-1)^{h-k}]\\+f_b\exp(i\varphi/2)\}.\end{aligned}$$

This means that neither diffuse scattering nor Bragg reflection can be observed along c^* except for reflections at $\varphi=2\pi p$, p being any integer. This equation is the same as equation (4) and agrees with the observation.

(2) For $h-k=3n\pm1$,

summation of the intensity equation (18) can be carried out when x_ν's and c_ν's are evaluated from equations (16) and (17). It is the sum of two terms which are expressed as

$$I=ND+H, \tag{20}$$

where

$$D=\sum_\nu c_\nu+\sum_\nu c_\nu\frac{x_\nu\exp(-i3\varphi)}{1-x_\nu\exp(-i3\varphi)}+\text{conjugate},$$

and

$$H=\sum_\nu c_\nu\frac{x_\nu^{N+1}\exp(-i3(N+1)\varphi)-x_\nu\exp(-i3\varphi)}{(1-x_\nu\exp(-i3\varphi))^2}+\text{conjugate}.$$

We call the first term the diffuse term and the second the higher term. In general $|x_\nu|<1$; therefore the higher term is negligible compared with the diffuse term since N is supposed to be very large.

The final formula for the diffuse term can be given by

$$D=\frac{\begin{aligned}\delta(1-\delta)\{2V_1^*V_1+\varepsilon^*V_1^*V_2+\varepsilon V_2^*V_1+2V_2^*V_2\\+2U_r\cos3\varphi-2U_i\sin3\varphi\}\end{aligned}}{\begin{aligned}1-2\delta+5\delta^2+4(1-\delta)^2\times\cos3\varphi\\+4(1-2\delta)\cos^2 3\varphi\end{aligned}} \tag{21}$$

where U_r and U_i are the real and imaginary parts of $(-\varepsilon V_1+\varepsilon^* V_2)(V_1^*-V_2^*)$ respectively. Intensity distributions along c^* are calculated by equation (21), and they are shown in Figs. 8 and 9 for 10ζ and 20ζ up to $\zeta=1$ at various values of the stacking fault probability, δ.†

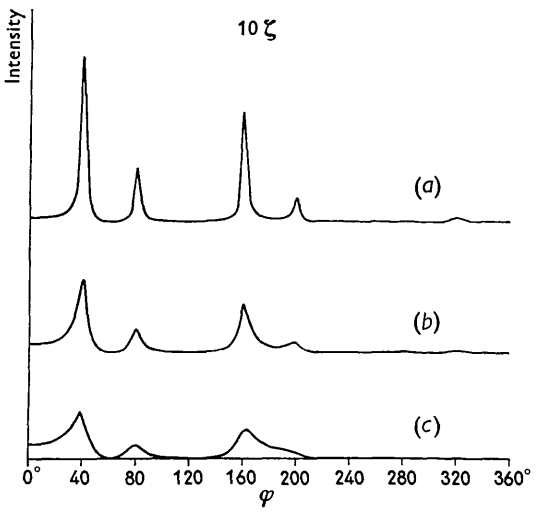

Fig. 8.

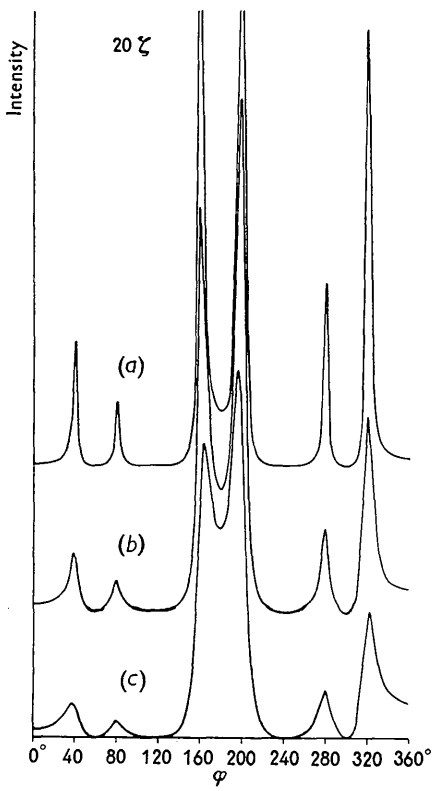

Fig. 9.

Figs. 8 and 9. Calculated intensity distributions along 10ζ and 20ζ row lines for the 9-layer structure with stacking faults, δ being the stacking fault probability. (*a*) $\delta=0{\cdot}1$. (*b*) $\delta=0{\cdot}2$. (*c*) $\delta=0{\cdot}3$.

(*b*) *Disordered stacking of two 5-layer sequences*

There are only two kinds of regular 5-layer sequences which can be constructed by the stacking of layers A, B, C, A', B' and C' if we obey the rule mentioned in Table 1. These are $ABCAB'$ and its reverse structure $AB'A'C'B'$. X-ray intensity formula due to the disordered stacking of these two structures is quite analogous with the example dealt with in the previous paper (refer to equation (42) of Kakinoki & Komura, 1952).

Thus derived intensity formula is

$$I=\tfrac{1}{4}(V_1^*+V_2^*)(V_1+V_2)\,(\sin^2 N'\tfrac{5}{2}\varphi/\sin^2\tfrac{5}{2}\varphi)$$
$$+\tfrac{1}{4}(V_1^*-V_2^*)(V_1-V_2)\{N'(1-x^2)/(1+x^2-2x\cos 5\varphi)$$
$$+\text{ higher term}\}, \qquad (22)$$

where $5N'=N_0$, $x=-(1-2\alpha)$, and α is the stacking fault probability of the sequence

$$ABCAB'-AB'A'C'B'-ABCAB'-\ldots;$$

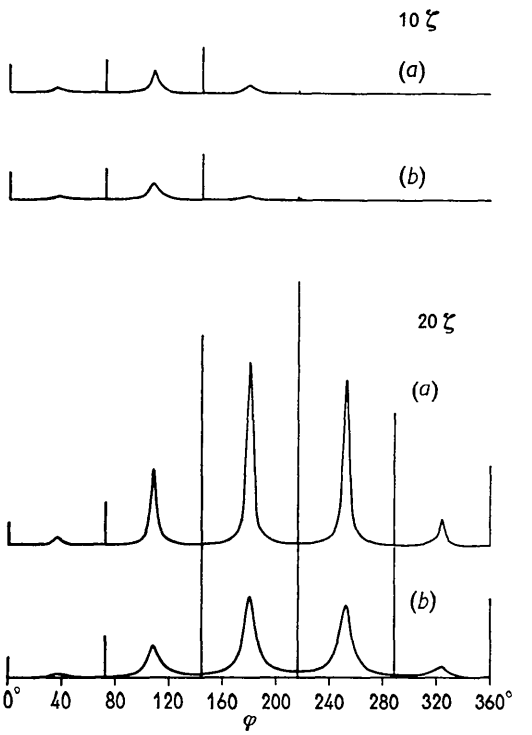

Fig. 10. Calculated intensity distributions along 10ζ and 20ζ row lines for the disordered stacking of two 5-layer sequences, α being the stacking fault probability. (*a*) $\alpha=0{\cdot}1$. (*b*) $\alpha=0{\cdot}2$.

† There is another way to calculate the diffuse term of equation (20) without solving equations (16) and (17). The idea is to use the relationship between the roots and the coefficients of the characteristic equation (16). This is particularly useful when the order of the characteristic equation becomes higher. The detail will be discussed in separate paper (Kakinoki, 1961).

i.e., $\alpha=0$ for 10-layer structure and $\alpha=1$ for a mixture of two 5-layer structures. The higher term in equation (22) can be neglected unless α is very close to zero. V_1 and V_2 are expressed in this case as follows:

$$V_1=V_A+V_B\exp(i\varphi)+V_C\exp(i2\varphi)+V_A\exp(i3\varphi)+V_{B'}\exp(i4\varphi)\,, \quad (23)$$

$$V_2=V_A+V_{B'}\exp(i\varphi)+V_{A'}\exp(i2\varphi)+V_{C'}\exp(i3\varphi)+V_{B'}\exp(i4\varphi)\,. \quad (24)$$

When $h-k=3n$, $V_1=V_2$, hence equation (22) turns to equation (4). Intensity distributions along 10ζ and 20ζ calculated from equation (22) are plotted in Fig. 10 for $\alpha=0{\cdot}1$ and $0{\cdot}2$. In these figures thick vertical lines show Laue functions in equation (22) in a somewhat arbitrary scale, because no information is available for the number of layers N', but this number cannot be large since the observed reflections of $\zeta=4/10$ and $6/10$ are rather diffuse.

Figs. 11 and 12 show comparisons between the observed and calculated intensity distributions. The calculated curves due to 9-layer sequence with stacking faults and the disordered stacking of two 5-layer sequences are drawn separately for convenience' sake in these figures as curves (*b*) and (*c*) respectively. The ratio of the contribution of both structures is adjusted, so that observed intensity may be compared directly with the calculated curves. Qualitative agreements between observed and calculated intensity distributions are satisfactory when the stacking fault parameters are taken as $\delta=0{\cdot}1$ for 9-layer sequence and $\alpha=0{\cdot}2$ for 5-layer sequences.

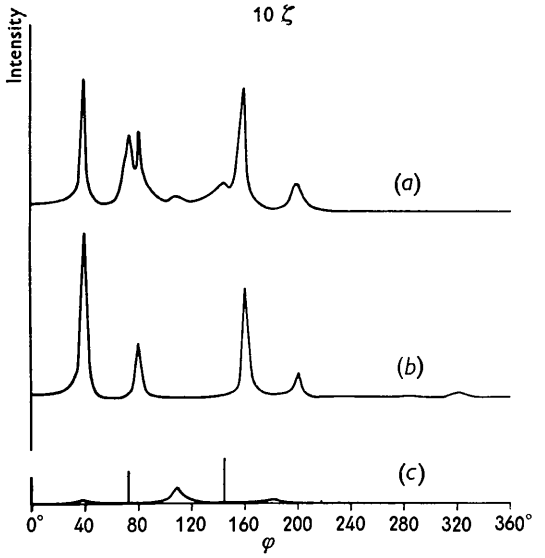

Fig. 11.

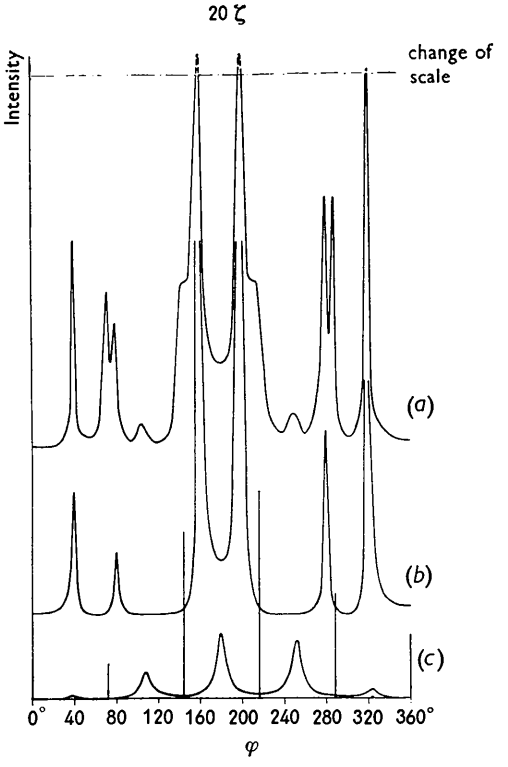

Fig. 12.

Figs. 11 and 12. Comparison of the observed and calculated intensity distributions of 10ζ and 20ζ row lines. (*a*) Observed curve. Bragg reflections due to the regular 4-layer structure are omitted in order to avoid unnecessary complication. (*b*) Calculated curve for the 9-layer sequence with stacking fault $\delta=0{\cdot}1$. (*c*) Calculated curve for the disordered stacking of two 5-layer sequences with $\alpha=0{\cdot}2$.

5. Discussion

Two new modifications having rhombohedral 9-layer ($a_0=12{\cdot}97$ Å, $\alpha=22°\,50'$, hexagonal lattice constants $a_0=5{\cdot}14$, $c_0=37{\cdot}89$ Å) and hexagonal 5-layer ($a_0=5.14$, $c_0=21{\cdot}05$ Å) sequences were found in the ternary Laves phase of MgCuAl in addition to the regular 4-layer structure. Fig. 13 shows these new structures based on the hexagonal cell, in which large white circles indicate the positions of magnesium atoms and small black circles show other metal positions. Diffuse scattering was also observed and satisfactorily interpreted as due to stacking faults related to two kinds of 9-layer sequences and due to the disordered stacking between two 5-layer sequences. Regarding the intensity distribution the theory of X-ray diffraction applied to close-packed structures was extended to the case in which there were two sets of layers, (A, B, C) and (A', B', C'). In this calculation an essential factor is how to combine these six layers to construct V_1 and V_2. For instance, the 2-layer structure is by no means obtained from any other combinations for V_1 and V_2 than those given in equations (11) and (12). With respect to this point a discussion will be made in a separate paper.

Many trials were needed in order to get the final result because the observed intensity distributions

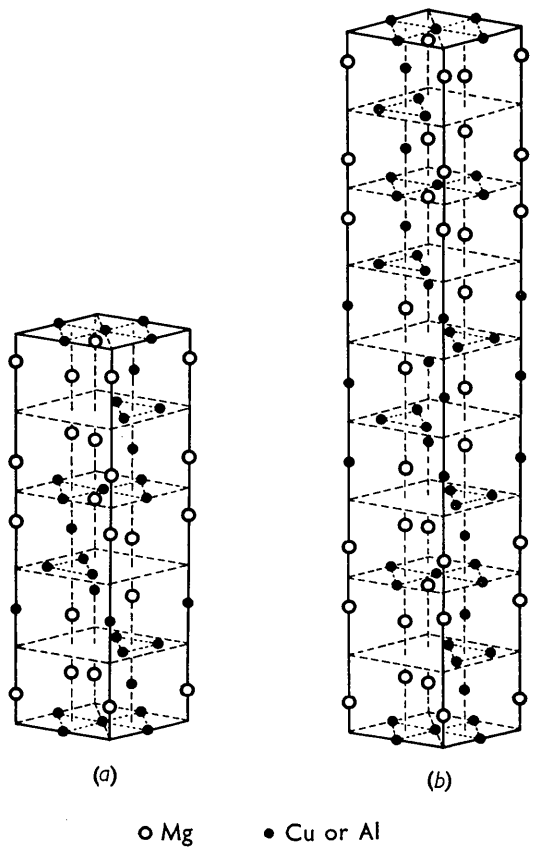

Fig. 13. The structure of two new modifications of the Laves phase, MgCuAl. (*a*) 5-layer type, *ABCAB'*. (*b*) 9-layer type, *AB'ABC'BCA'C*.

were so complicated that they could not be explained without considering the sample as a mixture of several kinds of crystallites with different structures mentioned above. The values of $\delta=0{\cdot}1$ and $\alpha=0{\cdot}2$ may have some allowance as can be inferred from the fact that other samples having approximately the same composition show a little different intensity distribution, as well as from the fact that there are still, in the present sample, slight discrepancies between observed and calculated intensity distribution. However, the results that faults are found among such kinds of coupled layers as shown in equation (7) and that the disorder occurred between V_1 and V_2 in equations (23) and (24) will not be changed.

There still remains a possibility of explaining the whole intensity distribution by an unified model in which the two modifications are combined. In this connection, the idea of the Fourier transformation of a diffuse line (Kakinoki, 1961) may be a helpful approach. Moreover, a sort of modulated structure similar to the case of the Cu–Ni–Fe alloys (Hargreaves, 1951) may occur in the present alloy too. But even so, other models which may be obtained cannot differ greatly from the model given here.

Considering complexity of the obtained structures there may be some other modifications even for the samples having approximately the same composition but it needs many more experiments to find out and confirm all possible modifications.

In the present paper no attention has been paid to the ordering of copper and aluminium atoms. It is possible to treat the effect of ordering, but very accurate estimates of the intensities of reflections should be required, and the experimental difficulties would be great. An attempt is in progress to control the degree of stacking faults by means of annealing the alloys in order to elucidate the nature of the stacking faults. Ordering of the copper and aluminium atoms might be discovered in the process of such experiments.

The author wishes to express his sincere thanks to Prof. J. Kakinoki of Osaka City University and Prof. T. Watanabé of Osaka University for their stimulating discussion and encouragements during the course of this study. He is also grateful to Dr M. Ohta for suggesting this problem. This work was supported by the Scientific Research Grant of the Ministry of Education of Japan.

References

Berry, R. L. & Raynor, G. V. (1953). *Acta Cryst.* **6**, 178.
Frank, F. C. & Kasper, J. S. (1959). *Acta Cryst.* **12**, 483.
Hargreaves, M. E. (1951). *Acta Cryst.* **4**, 301.
Hendricks, S. & Teller, E. (1942). *J. Chem. Phys.* **10**, 147.
Jagodzinski, H. (1949*a*). *Acta Cryst.* **2**, 201.
Jagodzinski, H. (1949*b*). *Acta Cryst.* **2**, 208.
Jagodzinski, H. (1949*c*). *Acta Cryst.* **2**, 298.
Jagodzinski, H. (1954). *Acta Cryst.* **7**, 17.
Kakinoki, J. & Komura, Y. (1952). *J. Phys. Soc. Japan*, **7**, 30.
Kakinoki, J. & Komura, Y. (1954*a*). *J. Phys. Soc. Japan*, **9**, 169.
Kakinoki, J. & Komura, Y. (1954*b*). *J. Phys. Soc. Japan*, **9**, 177.
Kakinoki, J. (1961). Private communication.
Laves, F. & Witte, H. (1936). *Metallwirtschaft*, **15**, 15.
Raynor, G. V. (1949). *Progress in Metal Physics*, Vol. 1. London: Butterworths Scientific Publications.
Wilson, A. J. C. (1942). *Proc. Roy. Soc.* A, **180**, 277.